Time Series Analysis of Air Pollutant Gas Concentrations: A Case Study in Isfahan's Urban Area

Fatemeh Esmaeili[1]*, Hamid Mehrabi[1]

[1] Department of Geomatics Engineering, Faculty of Civil Engineering and Transportation, University of Isfahan, Isfahan, Iran.

KEY WORDS: Air pollution, Nitrogen oxides, Ozone, Isfahan city, time series analysis, LS-HE

ABSTRACT:

Monitoring, documenting, and analysing atmospheric pollutant levels in urban areas are vital for understanding and mitigating their impacts on human health and ecosystems. Studying the temporal patterns of ozone (O_3) and nitrogen oxides (NO, NO_2, NOx)—the primary air pollutants—is especially important in air quality research. This study investigates the dominant variations of ozone and nitrogen oxides concentrations in Isfahan city. Data collected from air pollution stations from 2018 to 2024 were analyzed, focusing on O_3, NO, NO_2, and NOx levels. Least Squares Harmonic Estimation (LS-HE) analysis of the time series confirmed a significant annual harmonic pattern for O_3, NO, and NOx gases at a 99% confidence level. Additionally, the daily 24-hour cycle of the time series was identified. Lastly, the Pearson correlation coefficient was computed to assess the linear relationships among the studied variables. Results reveal an inverse annual relationship: peak O_3 levels occur in summer, while NO and NOx concentrations are at their lowest during this period. Daily patterns show O_3 peaking between 4:00 PM and 8:00 PM, coinciding with the lowest NO and NOx levels. Pearson correlation analysis indicates a weak, inverse linear relationship between NO_2 and O_3 concentrations. Additionally, some months in 2023 exhibited inconsistent daily patterns, highlighting complex dynamics in air pollution behaviors.

1. INTRODUCTION

Air pollution from photochemical oxidants has been on the rise in recent decades, particularly in urban areas (Notario et al., 2012). Industrial activities, population growth, and traffic contribute to elevated concentrations of tropospheric ozone (O3) and nitrogen dioxide (NO2). Monitoring changes in the levels of these pollutant gases is crucial for managing air quality and mitigating their harmful effects on residents' health. The number of days with high ozone concentrations in urban settings can have potentially adverse health effects. Exposure to air pollutants like ozone (O3), nitrogen dioxide (NO2), carbon monoxide (CO), and volatile organic compounds can harm the cardiorespiratory system and weaken the immune response, making individuals more susceptible to viral and bacterial infections (Martelletti and Martelletti, 2020). Zoran et al. (2020) has shown that increased levels of ozone (O3) and nitrogen dioxide (NO2) are linked to respiratory illnesses and the spread of viruses, including the coronavirus.

Ozone (O3) exists in both the Earth's upper atmosphere (stratosphere) and at the Earth's surface (troposphere). In the stratosphere, ozone acts as a protective barrier against harmful ultraviolet radiation. Conversely, at the surface, ozone is a secondary air pollutant formed through complex photochemical reactions involving solar radiation, nitrogen oxides (NO_x), and volatile organic compounds (VOCs) (Seinfeld and Pandis 2016). Therefore, investigating the relationship between ozone concentrations and nitrogen oxide gases is important in studying air pollutants. Nitrogen oxide (NOx) is produced from the chemical combination of nitric oxide (NO) and nitrogen dioxide (NO2) (NO+NO2=NOx). Photochemical processes influenced by emissions of nitrogen oxide (NOx) gas and volatile organic compounds cause tropospheric O3 levels to increase significantly. However, due to the surface chemical coupling of O3 and NOX, the response of increasing O3 gas to decreasing NOX emissions is not linear (Mazzeo et al., 2005).

The primary objective of this study is to investigate the impact of nitrogen oxide gases on the increasing concentrations of ozone (O3) in Isfahan. The analysis utilizes hourly time series data of ozone, nitric oxide (NO), nitrogen dioxide (NO2), and nitrogen oxides (NOx) collected from the 25 Aban Square station along Kaveh Boulevard. Notably, these time series contain missing data spanning over six months during the study period. Thus, selecting an appropriate time series analysis method capable of handling this missing data is crucial for examining trends and changes over the six years.

In this study, we analyzed time series data related to ozone and nitrogen oxides concentrations using the least squares harmonic estimation (LS-HE) method. A key advantage of the LS-HE method over other common time series analysis techniques, such as Fast Fourier Transform (FFT) and Singular Spectrum Analysis (SSA), is that it does not require input data to be equally spaced. When fitting harmonics or polynomial models to fill data gaps, interpolation methods can introduce errors in subsequent analyzes. In contrast, the LS-HE method maximizes the use of the original time series data without interpolation biases.

The LS-HE method is a parametric approach for analyzing the harmonic behaviors of time series. Initially implemented by Amiri Simkooei on GNSS station time series, this method aims to reconstruct the harmonic behaviors of these series by modeling harmonic functions (Amiri-Simkooei et al., 2007). It was developed in a multivariate mode and has since been widely applied in the analysis of GPS station time series, facilitating the discovery of frequencies associated with these series(Amiri-Simkooei, 2020; Amiri-Simkooei 2009; Amiri-Simkooei and Tiberius, 2007; Amiri-Simkooei, 2013).

The effectiveness of the LS-HE method in time series analysis has been demonstrated in numerous applications involving GNSS, sea level measurements and total electron content (TEC) data analysis. The application of the multivariate LSHE has led to the identification of the precise frequency and period of the Draconic signal in GNSS station time series (Amiri-Simkooei,

* Corresponding author (Fatima.esmaeili74@gmail.com)

2013). Additionally, the LSHE method has been utilized to analyze and uncover harmonic behaviors in sea level data (Amiri-Simkooei et al., 2014), as well as in the examination of TEC time series in the Earth's atmosphere (Amiri-Simkooei and Asgari, 2012).

In this research, Section 2 briefly explains the LSHE method and the correlation coefficient parameter. Section 3 introduces the input time series data used for interannual and daily analyzes. Section 4 presents the results of analyzing the behavior of the time series over long-term (interannual changes) and short-term (daily changes) periods. Finally, Section 5 discusses the conclusions regarding the patterns of change in ozone and nitrogen oxides concentrations and their relationship.

2. METHODS

Subsections 2.1 of this section provide a brief overview of the LS-HE time series analysis method, while subsection 2.2 discusses the Pearson correlation coefficient and its statistical interpretation.

2.1 Least Square Harmonic Estimation (LS-HE)

Let $\boldsymbol{y}(t_{i=1,\dots,m})$represent a time series of length m. To estimate the unknown parameters of this time series (number of unknown parameters: n), we can formulate the following linear model:

$$\mathrm{E}(\boldsymbol{y}) = \boldsymbol{A}\boldsymbol{x}, \qquad \mathrm{D}(\boldsymbol{y}) = \boldsymbol{Q}_{\boldsymbol{y}} \tag{1}$$

Where $\boldsymbol{A}$ is the design matrix with dimensions $m \times n$. $\boldsymbol{y}$ is a vector of observations of length m, and $\boldsymbol{x}$ is a vector of unknown parameters of length n. The number of unknown parameters n, along with the dimensions and elements of matrix $\boldsymbol{A}$, is determined based on specific assumed behaviors of the time series $\boldsymbol{y}$.

The functional model $\mathrm{E}(\boldsymbol{y}) = \boldsymbol{A}\boldsymbol{x}$ can represent either a specific linear behavior or, in the context of harmonic estimation, linear behavior plus p periodic signals (Amiri-Simkooei and Asgari 2012). In the latter case, each observation epoch can be rewritten as follows:

$$\boldsymbol{y}(t_i) = \varepsilon + \beta t_i + \sum_{k=1}^{p} a_k \cos(\omega_k t_i) + b_k \sin(\omega_k t_i) \tag{2}$$

ε is the initial shift value of the data, β is the long-term linear rate of change, a_k and b_k are the unknown coefficients for the k-th signal. Therefore, the design matrix $\boldsymbol{A}$ is formed as follows:

$$\boldsymbol{A} = \begin{bmatrix} 1 & t_1 & \cos(\omega_1 t_1) & \sin(\omega_1 t_1) & \dots \\ \vdots & \vdots & \vdots & \vdots & \\ 1 & t_m & \cos(\omega_1 t_m) & \sin(\omega_1 t_m) & \cdots \end{bmatrix} \tag{3}$$

To test for the presence or absence of ω_j frequency in the time series, the first step involves forming the design matrix $\boldsymbol{A}_j$ based on the assumption of a single harmonic behavior at frequency ω_j. The spectral power value for this frequency is calculated after least squares estimation using $\mathrm{p}(\omega_j) = \hat{\boldsymbol{e}}_0 \boldsymbol{Q}_{\boldsymbol{y}}^{-1} \boldsymbol{A}_j (\boldsymbol{A}_j^T \boldsymbol{Q}_{\boldsymbol{y}}^{-1} P_{\boldsymbol{A}}^{\perp} \boldsymbol{A}_j)^{-1} \boldsymbol{A}_j^T \hat{\boldsymbol{e}}_0$. In this equation, $\hat{\boldsymbol{e}}_0 = P_{\boldsymbol{A}}^{\perp} \boldsymbol{y}$ represents the least squares residual, and $P_A^{\perp} = \boldsymbol{I} - \boldsymbol{A}_j \left(\boldsymbol{A}_j{}^T \boldsymbol{Q}_{\boldsymbol{y}}^{-1} \boldsymbol{A}_j\right)^{-1} \boldsymbol{A}_j{}^T \boldsymbol{Q}_{\boldsymbol{y}}^{-1}$ is the perpendicular projector. To create the power spectrum, the power value for each frequency, $\mathrm{p}(\omega_j)$, is calculated.

For pollutant gas concentration data with a daily sampling rate over a period of 6 years, the frequency values $\omega_j = 2\pi n / 365.25 : n = 2 : 1 : 6 \times 365.25$ are used. The peaks in the power spectrum indicate the potential frequencies present in the time series. The largest peak corresponds to the frequency of the dominant harmonic behavior in the time series.

After confirming the significance of a frequency ω_k, the unknown coefficients for harmonic behavior are calculated using least squares theory from $\hat{\boldsymbol{x}} = \left(\boldsymbol{A}_k{}^T \boldsymbol{Q}_{\boldsymbol{y}}^{-1} \boldsymbol{A}_k\right)^{-1} \boldsymbol{A}_k{}^T \boldsymbol{Q}_{\boldsymbol{y}}^{-1} \boldsymbol{y}$. The amplitude of the signal can be calculated using $Am_k = \sqrt{a_k{}^2 + b_k{}^2}$.Based on least squares theory, the harmonic behavior of the time series can be reconstructed from $\hat{y} = \boldsymbol{A}_k \hat{x}$.

2.2 Wavelet scalogram

The Continuous Wavelet Transform (CWT) provides a time–frequency representation of a signal by correlating it with scaled and translated versions of a mother wavelet $\psi(t)$. Unlike the Fourier transform, which decomposes a signal into infinite-duration sinusoids, the CWT uses wavelets that are localized in both time and frequency, enabling analysis at all possible scales and positions. For a time series y(t), the CWT is defined as:

$$W(a,b) = (1/\sqrt{|a|}) \int_{-\infty}^{+\infty} y(t)\, \psi\left(\tfrac{t-b}{a}\right) dt \tag{4}$$

where $a > 0$ is the scale parameter (inversely related to frequency) and b is the translation parameter (time localization). The result, $W(a,b)$, constitutes how well the signal matches the dilated and translated wavelet, providing a redundant but highly informative representation.

In wavelet analysis, the scalogram is a representation that captures how the power of a signal is distributed across different frequencies. It uses wavelet scales, which correspond to dilation of the mother wavelet. The power at a given scale a is obtained by aggregating the squared magnitudes of the coefficients across time. A common measure is:

$$P(a) = \int_{-\infty}^{+\infty} |W(a,b)|^2 \, db \tag{5}$$

The scalogram is then the function $P(a)$.

2.3 Pearson correlation coefficient

The correlation coefficient between two variables serves as a quantitative measure of their linear dependence. Specifically, when each variable has N scalar observations, the Pearson correlation coefficient is defined as (Pearson 1895):

$$\rho(A,B) = \frac{1}{N-1} \sum_{i=1}^{N} \left(\frac{A_i - \mu_A}{\sigma_A}\right)\left(\frac{B_i - \mu_B}{\sigma_B}\right) \tag{6}$$

μ_A and σ_A represent the mean and standard deviation of variable A, while μ_B and σ_B denote the mean and standard deviation of variable B, respectively. The correlation coefficient matrix for these two variables displays the correlation coefficients for all possible pairwise combinations between them.

$$R = \begin{bmatrix} \rho(A,A) & \rho(A,B) \\ \rho(B,A) & \rho(B,B) \end{bmatrix} \tag{7}$$

Since A and B are perfectly correlated, the elements along the diagonal elements of this matrix are always equal to 1.

$$R = \begin{bmatrix} 1 & \rho(A,B) \\ \rho(B,A) & 1 \end{bmatrix} \quad (8)$$

The Pearson correlation coefficient is a statistical measure that quantifies the strength and direction of the linear independence between two variables, with values ranging from -1 to 1.

- **1**: Indicates a perfect positive correlation, meaning that an increase in one variable results in an increase in the other.
- **0**: Indicates independence, signifying that there is no relationship between the variables.
- **-1**: Indicates a perfect negative correlation, meaning that an increase in one variable results in a decrease in the other.

3. DATA SET

Currently, 13 monitoring stations are active in Isfahan to record pollutant gases, with their locations shown in Fig. 1. Of these, only five stations have recorded nitrogen oxides concentrations at various time intervals, and only the 25 Aban Square station on Kaveh boulevard is equipped with an ozone (O_3) analyzer. The average NOx concentration over a one-year period for these five stations is indicated by color labels in Fig. 1, with Feyz station exhibiting the highest average. Due to substantial missing data, a comprehensive assessment of the spatial pattern of gas concentrations is not feasible. Consequently, the analysis in the remainder of the study concentrates on data from the 25 Aban station.

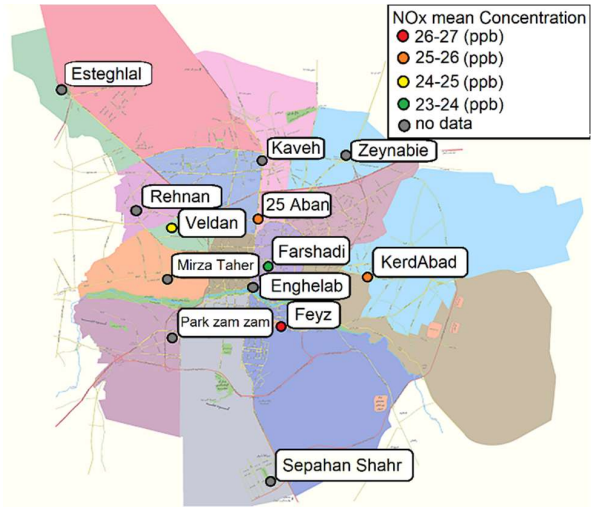

Figure 1. Locations of 13 air-pollution monitoring stations, color-coded by average NOx concentration.

This study analyzes time series data of ozone (O_3), nitric oxide (NO), nitrogen dioxide (NO_2), and nitrogen oxide (NO_x) concentrations. The data were recorded hourly at the 25 Aban Square station, covering the period from March 21, 2018, to March 19, 2024. Figure 2 presents the original time series data: ozone gas concentration (Fig. 2a), nitrogen oxide (Fig. 2b), nitric oxide (Fig. 2c), and nitrogen dioxide (Fig. 2d), represented as grey dots.

All time series analyzed in this study contain missing data. For the nitrogen oxides concentration time series, gaps occur from 2018 to mid-2019 and during the second half of 2020 (Fig. 2b, c, d). In contrast, the ozone (O_3) concentration time series only has missing data during the second half of 2020 (Fig. 2a). Typically, gaps in time series data are filled using interpolation methods, which can introduce biases in the estimation of linear and harmonic behavior (Lecomte et al. 2024). A key advantage of using the LS-HE method for analysing the time series in this research is that it does not require the input data to be evenly spaced.

The blue dots in Fig. 2 represent the daily moving average of the original data. In long-term time series analysis, applying the moving average technique helps mitigate the effects of excessive data sampling, providing a clearer view of long-term trends (Kumar et al. 2020). The daily moving average has also been utilized by Zoran et al. (2020) to analyze time series of ozone and nitrogen dioxides concentrations. This study analyzes time series data of ozone and nitrogen oxides concentrations to examine both long-term behaviors (annual changes) and short-term behaviors (daily changes). For the analysis of daily behaviors, the input consists of the original hourly time series data (grey dots in Fig.2). To detect and reconstruct interannual behaviors, the input data is derived from the daily moving average (blue dots in Fig.2).

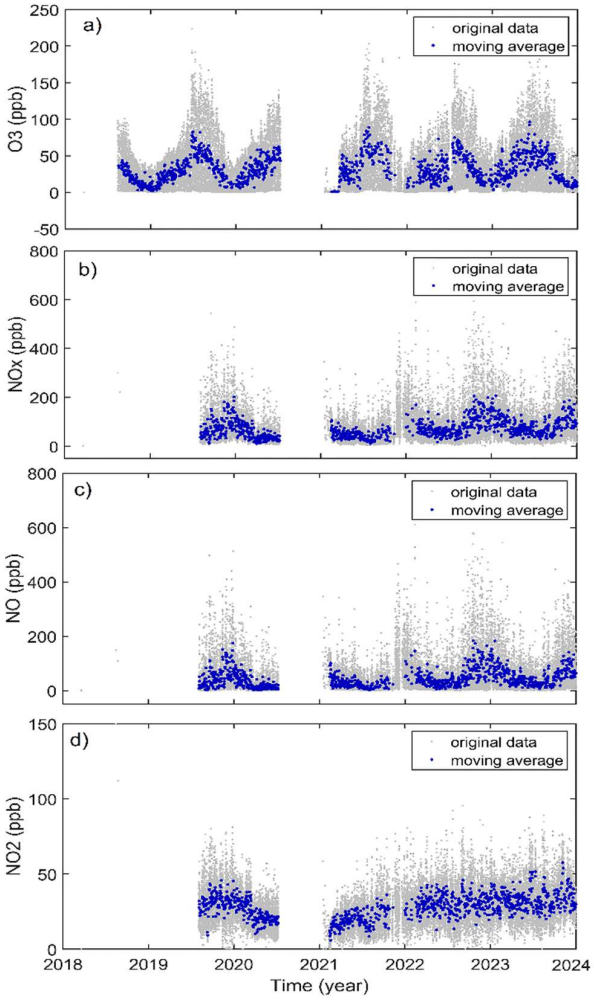

Figure 2. Time series data for ozone (a) gas concentrations, nitrogen oxide(b), nitric oxide(c), and nitrogen dioxide (d) with hourly rates (grey dots) and daily moving average data (blue dots).

4. RESULTS

To investigate the annual harmonic behavior of ozone and nitrogen oxides concentrations, analysis of the relevant data series was conducted using the LS-HE method. The results are

detailed in Subsection 4.1. The analysis of daily patterns in the concentration changes of these gases is presented in Subsection 4.2. In Subsection 4.3, the Pearson correlation coefficient between the examined time series is calculated to assess the linear relationship between ozone and nitrogen oxides concentrations in the air pollution data for the city of Isfahan.

4.1 Harmonic analysis of Ozone and Nitrogen Oxides concentrations time series

After applying a linear trend to the functional model of the time series, the power spectrum resulting from harmonic analysis of ozone (O_3), nitric oxide (NO), nitrogen dioxide (NO_2), and nitrogen oxide (NO_x) concentrations were generated based on the methodology outlined in Section 2, Fig. 3. The peaks highlighted in Figure 3 correspond to harmonic behaviors with a prominent semi-annual period (~170 days), all identified at the 99% confidence level for the O_3 (Fig. 3a), NO_2 (Fig. 3b), NO (Fig. 3c), and NOx (Fig. 3d) time series.

For the three gases, O_3, NO, and NO_x, the most prominent harmonic behavior is the annual behavior (period of approximately 360–365 days), as shown in Fig. 3 (a, c, d). The peak corresponding to this annual harmonic exhibits the highest power value in their LS-HE power spectrum. In contrast, the power spectrum for NO_2 shows the highest power at a periodicity of approximately 1382 days (about 4 years). However, considering the study period of six years and the fact that over one year of data is missing, this peak is likely related to the length of the time series rather than a significant periodic phenomenon.

Other confirmed peaks in the power spectrum of O_3, NO, and NO_x gases may result from modulation (amplitude variations) of the annual harmonic behavior. Changes in the amplitude of a harmonic can produce peaks on either side of the main peak in the spectrum (Amiri-Simkooei and Asgari 2012). To compare the amplitude variations of the annual harmonic across different years, the amplitude for the three pollutants, O_3, NO, and NO_x were estimated, Table 1. The hatched cells indicate years where amplitude estimations are unreliable due to a high volume of missing data. According to Table 1, the amplitude of the annual cycle for O_3 was highest in 2021 and lowest in 2019. For NO and NO_x, the amplitudes in 2022 and 2023 were greater than those in 2019 and 2021.

Pollutant gas	2018	2019	2020	2021	2022	2023
O3	23.5	10.6		27.0	16.7	20.4
NO		17.9		19.8	31.3	30.7
NOx		18.5		25.8	29.9	30.9

Table 1. Amplitude of the annual variation in O_3, NO, and NO_x pollutant gas concentrations.

Fig. 3 displays the reconstructed annual harmonic behavior for the concentrations of O_3, NO, and NO_x in 2019, 2022, and 2023. Reconstructing this harmonic for 2018, 2020, and 2021 is not feasible due to the substantial amount of missing data. An important point in analyzing and interpreting this reconstruction is that the estimated amplitude does not represent the maximum or minimum values observed in that year; instead, it reflects the range of variation throughout the year.

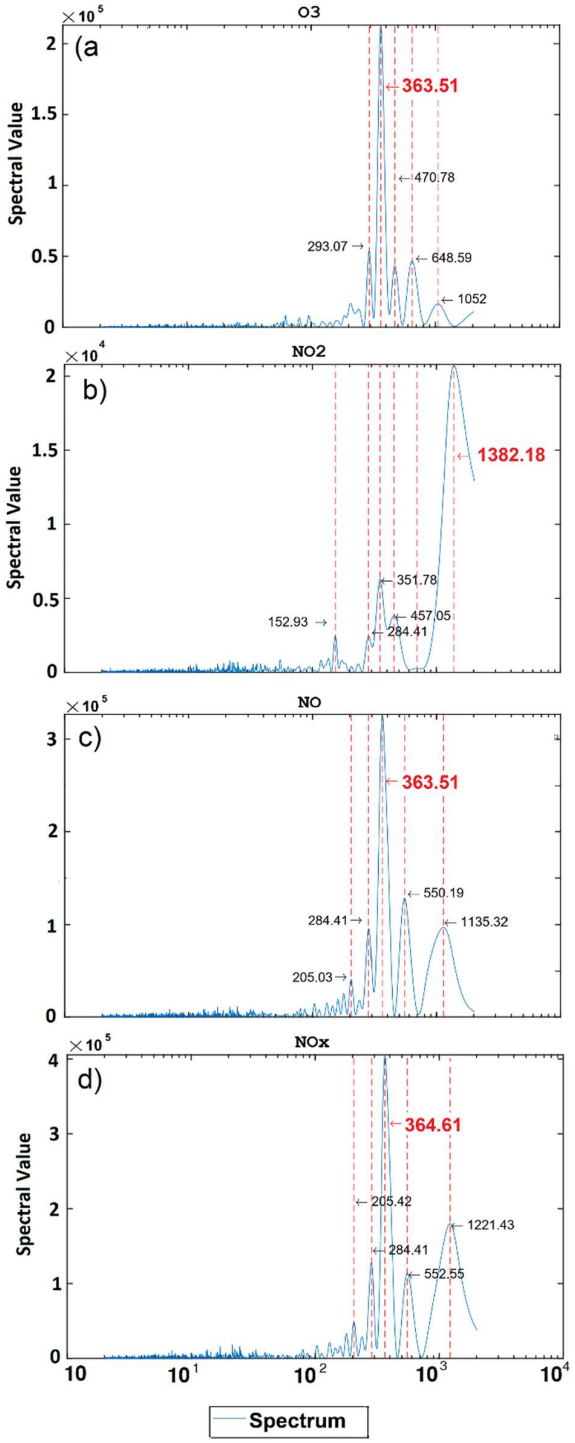

Figure 3. LS-HE power spectrum of ozone (a) gas concentrations, nitrogen dioxide (b), nitric oxide(c), and nitrogen oxide (d)

According to the results in Fig. 4, the pattern of annual variation in ozone concentration shows that levels are low during the winter months at the start of the year. The concentration then gradually increases, reaching a peak around the middle of the year (summer months), and decreases again afterward. In 2023, the maximum O_3 concentration occurs in June, while in 2019 and 2022, it peaks in July and August, respectively.

The annual variation pattern for NO and NO_x concentrations shows higher levels at the beginning of the year (winter months), which then decrease as summer approaches. The lowest concentrations for both gases are observed in July across all years (Fig. 5, 6). In 2019, the concentration time series for NO and NO_x contain significant missing data, primarily in the first half of the year. Therefore, the annual signal fitting and amplitude estimation were performed based on the data from the second half of the year (Fig. 5 and 6, top).

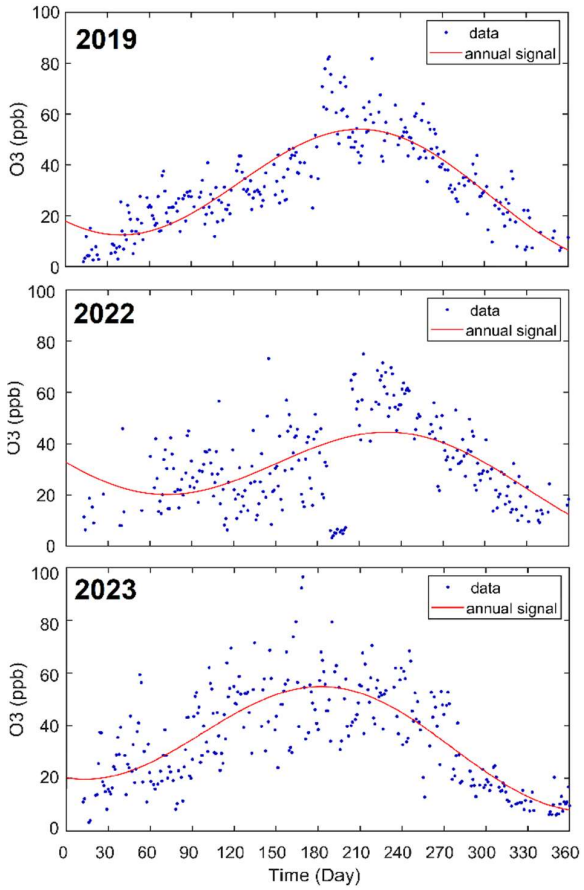

Figure 4. Daily moving average data O_3 (blue dots) and their annual harmonic patterns are shown for the years 2019 (top), 2022 (middle), and 2023 (bottom).

4.2 Analysis of Daily Variations in Ozone and Nitrogen Oxides Concentrations

To clarify the daily variation patterns of ozone (O_3) and nitrogen oxide (NO_x), their daily concentration changes for 2019, 2022, and 2023 are illustrated in Figs. 7, 8. Due to significant missing data in 2020 and 2021, reconstructing their change patterns is not feasible. The daily behavior patterns of nitric oxide (NO) and nitrogen oxide (NOx) concentrations are quite similar. As noted later in Section 4.4, the time series for these two gases are highly correlated, so the frames in Fig. 8 for gas NOx is similar to that for gas NO. Additionally, the daily variations in nitrogen dioxide (NO_2) showed no specific behavior, which is why NO_2 and NO results were not included in this study's results.

Regarding the 24-hour variation in O_3 concentration, most days show a pattern where levels are low during the early hours (midnight to early morning), then peak between 4-8 p.m., and decrease afterward, Fig 7. The lowest concentrations typically occur between 9 a.m. and 12 p.m. In 2023, this pattern differs in some months (June, July, August, and October), which warrants further investigation in future research.

Based on Fig. 8, the daily pattern of NO_x concentration typically shows two peaks: one between 9 a.m. and 12 noon, and another between 9 p.m. and 12 a.m. This contrasts with the daily variation pattern of O_3 concentration. In 2023, the NO_x daily variation differs from that in 2019 and 2022, especially in some months such as June, July, August, and October, where the patterns are notably distinct.

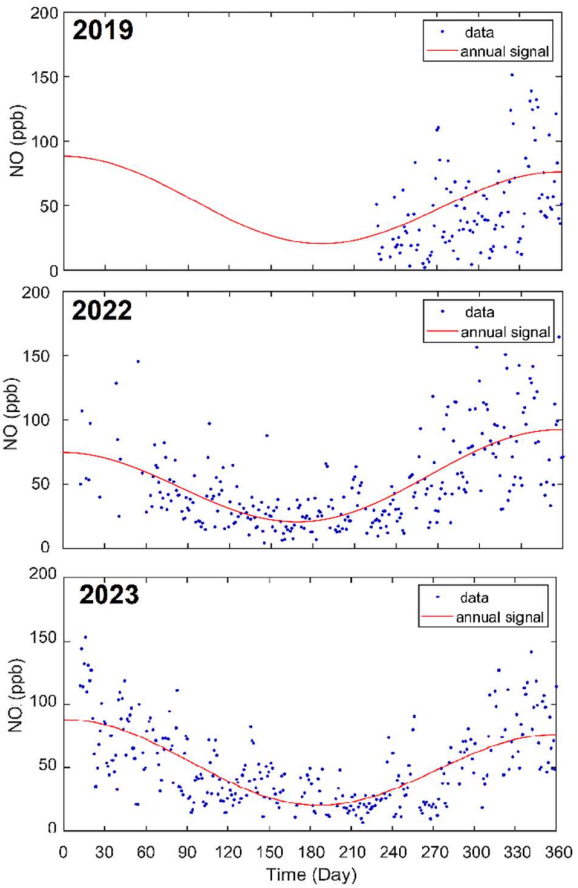

Figure 5. Daily moving average data NO (blue dots) and their annual harmonic patterns are shown for the years 2019 (top), 2022 (middle), and 2023 (bottom).

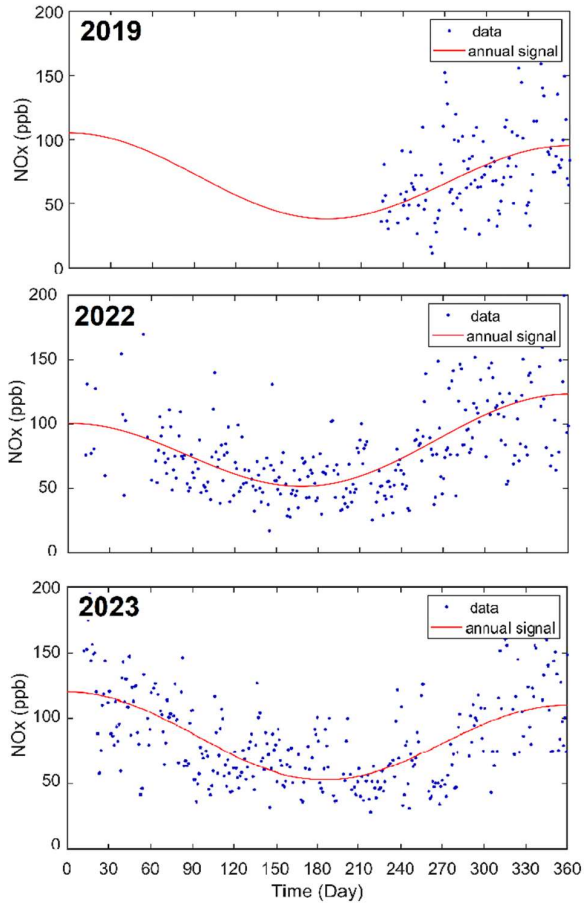

Figure 6. Daily moving average data NO_x (blue dots) and their annual harmonic patterns are shown for the years 2019 (top), 2022 (middle), and 2023 (bottom).

4.3 Validation of results based on wavelet scalogram

Using the continuous wavelet transform (CWT) method described in Section 2.2 requires the data to be evenly spaced. Due to the studied time spans and missing data, the wavelet scalogram could be generated only for the O_3 gas time series in the years 2019, 2022, and 2023. Figure 9 demonstrates a daily behavior (frequency 1 cycle per day) in the O_3 concentration time series. The prominence of this daily cycle is evident in the scalograms for all three years (2019, 2022, 2023), particularly during the summer months. These scalogram results corroborate the findings from Fig. 4 and 7, which were obtained using the LS-HE method.

4.4 Linear correlation between ozone gas concentrations and nitrogen oxides

In Section 2.2, the Pearson correlation coefficient was described as a statistical tool to assess the strength and direction of linear relationships between two variables, with its mathematical formula also provided. In this study, correlation coefficients between the time series of ozone (O_3), nitric oxide (NO), nitrogen dioxide (NO_2), and nitrogen oxide (NO_x) concentrations were calculated. Table 2 presents the numerical values of these coefficients. The results show that NO and NO_x concentrations are highly and positively correlated (coefficient: 0.978), indicating a strong direct relationship. NO_2 concentrations are most strongly linked to NO_x (coefficient: 0.639). Conversely, the correlation between O_3 and all nitrogen oxides is negative, meaning an increase in one lead to a decrease in the other. Specifically, O_3 concentration has a moderate negative correlation with NO and NO_x (coefficient: -0.43), and a weak negative correlation with NO_2 (coefficient: -0.195).

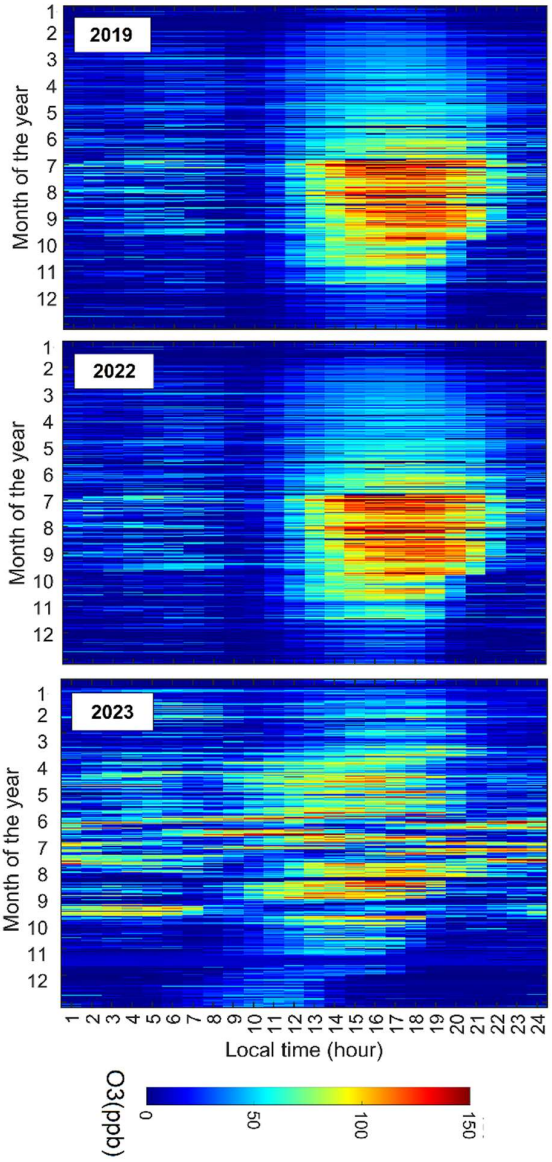

Figure 7. Daily patterns of ozone O_3 concentration changes during 24 hours for the years 2019, 2022, and 2023.

correlation	O3	NO	NO2	NO_x
O3	1.000	-0.439	-0.195	-0.427
NO	-0.439	1.000	0.468	0.978
NO2	-0.195	0.468	1.000	0.640
NO_x	-0.427	0.978	0.640	1.000

Table 1. Correlation coefficients between the time series of pollutant gases: NO_2, NO, NO_x, and O_3.

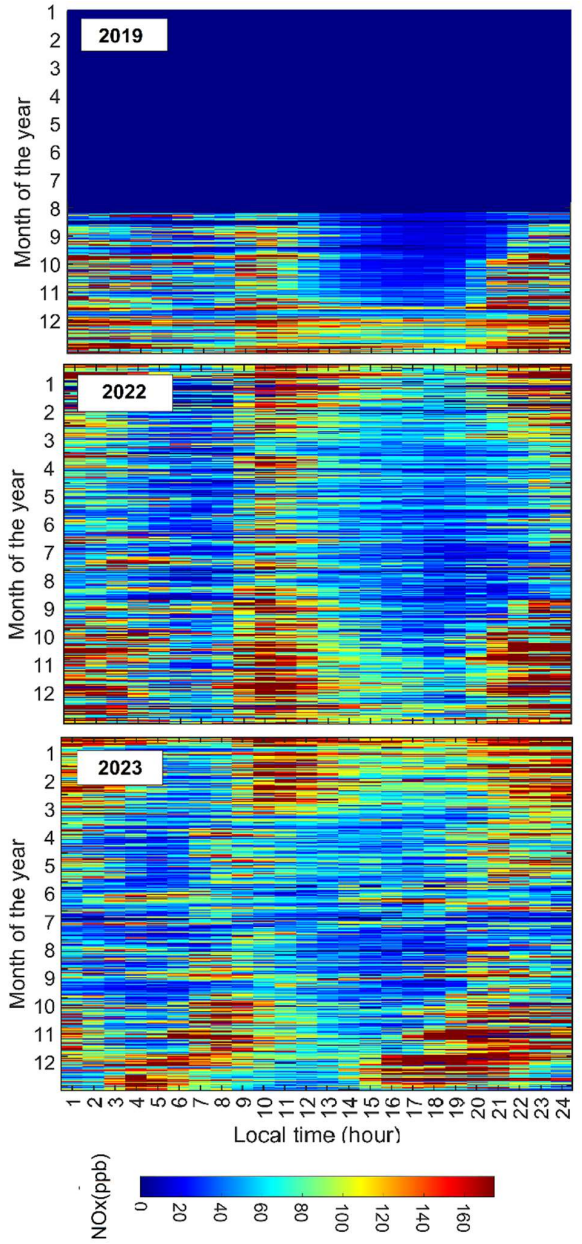

Figure 8. Daily patterns of ozone NO_x concentration changes during 24 hours for the years 2019, 2022, and 2023.

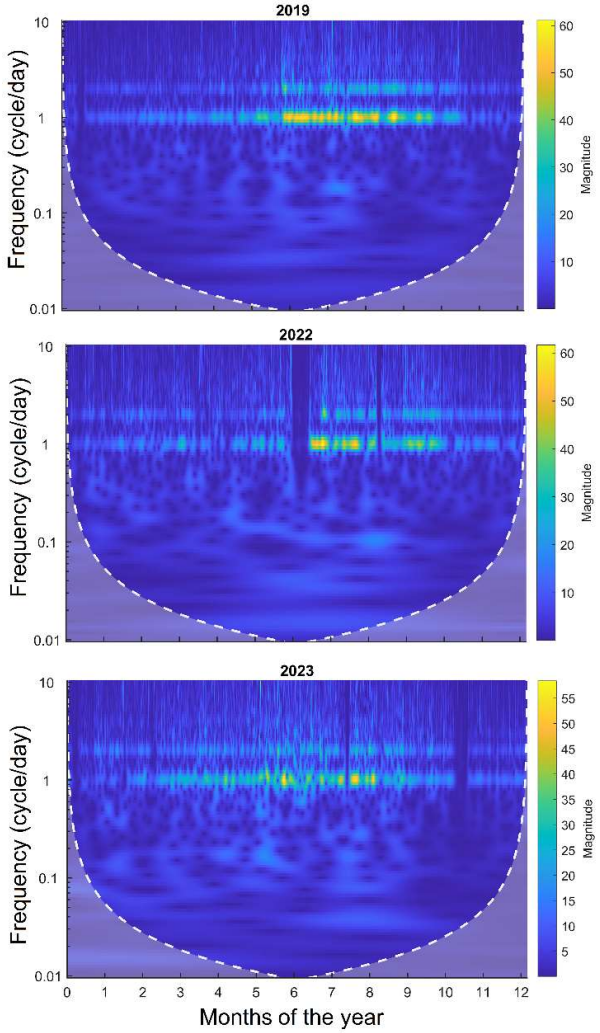

Figure 9. wavelet scalogram of O_3 concentration time series for the years 2019, 2022, and 2023.

5. CONCLUSIONS

The primary objective of this research was to examine the patterns of concentration changes in ozone (O_3), nitric oxide (NO), nitrogen dioxide (NO_2), and nitrogen oxide (NO_x) gases, and to explore the relationships among these pollutants in Isfahan. To achieve this, the concentration time series were analyzed for their annual and daily variation patterns, and linear correlations between these series were calculated. Additionally, to understand the harmonic behaviors, the power spectrum of these gases' concentrations was generated using the least squares harmonic estimation (LS-HE) method. A key advantage of LS-HE over other time series analysis techniques is that it does not require data to be evenly spaced, making it particularly suitable for analysing pollutant data from Isfahan, which contains significant missing values. The results of long-term (annual), short-term (daily) analyzes, and the correlation coefficients calculation of the time series are summarized below:

- The dominant harmonic pattern in the time series of NO_x, O_3, and NO concentrations is the annual signal.
- Annual oscillations in O_3 concentrations show low levels during the winter months at the start of the year, gradually increasing to a maximum in the summer

months, and then decreasing again towards the end of the year.

- The annual pattern of NO and NO_x concentrations shows higher levels at the beginning of the year (winter months), followed by a decrease as summer approaches, with concentrations increasing again toward the end of the year.
- Over a 24-hour period, O_3 concentrations are lowest during the early hours (midnight and morning), increase steadily to reach a maximum between 4 and 8 p.m., and then decrease again.
- Validation of the results was performed by generating a wavelet scalogram for the O_3 gas concentration time series in 2019, 2022, and 2023. The analysis confirms the daily behavior pattern in O_3 concentration changes and highlights the prominence of this behavior during the summer months in the studied years.
- The daily variation pattern of NO_x concentrations is similar to that of NO, with peak levels occurring during the day between 9 a.m. and 12 noon, and again between 9 p.m. and 12 a.m.
- NO_x concentrations take longer to decrease from their peak to their lowest levels compared to NO.
- Changes in NO and NO_x concentrations are highly and directly correlated (correlation coefficient of 0.978).
- NO_2 concentrations are most strongly dependent on NO_x levels, with a correlation coefficient of 0.639.
- The correlation between O_3 and all nitrogen oxides is negative, indicating that an increase in one corresponds to a decrease in the other.
- -O_3 concentrations have a moderate inverse relationship with NO and NO_x (correlation coefficient of -0.43) and a weak inverse relationship with NO_2 (correlation coefficient of -0.195).

ACKNOWLEDGEMENTS

We thank the Isfahan Municipality for providing the data recorded at the city's air pollution monitoring stations.

REFERENCES

Amiri-Simkooei Alireza., 2020: Least Squares Contribution to Geodetic Time Series Analysis Geodetic Time Series Analysis in Earth Sciences. 185-209

Amiri-Simkooei AR., 2009: Noise in multivariate GPS position time-series Journal of Geodesy. 83:175-187

Amiri-Simkooei AR, Asgari J., 2012: Harmonic analysis of total electron contents time series: methodology and results GPS solutions. 16:77-88

Amiri-Simkooei AR, Tiberius CCJM., 2007: Assessing receiver noise using GPS short baseline time series GPS solutions. 11:21-35

Amiri-Simkooei AR, Tiberius Christian CJM, Teunissen Peter JG., 2007: Assessment of noise in GPS coordinate time series: methodology and results Journal of Geophysical Research: Solid Earth. 112.

Amiri-Simkooei AR, Zaminpardaz Safoora, Sharifi MA., 2014: Extracting tidal frequencies using multivariate harmonic analysis of sea level height time series Journal of geodesy. 88:975-988

Amiri-Simkooei AR., 2013: On the nature of GPS draconitic year periodic pattern in multivariate position time series Journal of Geophysical Research: Solid Earth. 118:2500-2511

Kumar Anumandla Kiran, Lakshmi A Sri, Rao P Janaki Nivas., 2020: Moving average method based air pollution monitoring system using IoT platform. Journal of Physics: Conference Series.

Lecomte Hugo, Rosat Severine, Mandea Mioara, 2024: Gap filling between GRACE and GRACE-FO missions: assessment of interpolation techniques Journal of Geodesy. 98:1-19

Martelletti Luigi, Martelletti Paolo., 2020: Air pollution and the novel Covid-19 disease: a putative disease risk factor SN comprehensive clinical medicine. 2:383-387

Mazzeo Nicolás A, Venegas Laura E, Choren Hipólito, 2005: Analysis of NO, NO2, O3 and NOx concentrations measured at a green area of Buenos Aires City during wintertime Atmospheric Environment. 39:3055-3068

Notario Alberto, Bravo Iván, Adame José Antonio, Díaz-de-Mera Yolanda, Aranda Alfonso, Rodríguez Ana, Rodríguez Diana, 2012: Analysis of NO, NO2, NOx, O3 and oxidant (OX= O3+ NO2) levels measured in a metropolitan area in the southwest of Iberian Peninsula Atmospheric Research. 104:217-226

Pearson Karl., 1895: VII. Note on regression and inheritance in the case of two parents proceedings of the royal society of London. 58:240-242

Seinfeld John H, Pandis Spyros N., 2016: Atmospheric chemistry and physics: from air pollution to climate change. John Wiley & Sons.

Zoran Maria A, Savastru Roxana S, Savastru Dan M, Tautan Marina N., 2020: Assessing the relationship between ground levels of ozone (O3) and nitrogen dioxide (NO2) with coronavirus (COVID-19) in Milan, Italy Science of The Total Environment. 740:140005